Published in final edited form as:
J Mol Biol. 2010 March 12; 396(5): 1244–1259. doi:10.1016/j.jmb.2010.01.013.

The crystal structure and activity of a putative trypanosomal nucleoside phosphorylase reveal it to be a homodimeric uridine phosphorylase

Eric T. Larson[a,b], **Devaraja G. Mudeppa**[c], **J. Robert Gillespie**[d], **Natascha Mueller**[a,b], **Alberto J. Napuli**[a,b], **Jennifer A. Arif**[d], **Jenni Ross**[a,b], **Tracy L. Arakaki**[a,b], **Angela Lauricella**[e], **George DeTitta**[e], **Joseph Luft**[e], **Frank Zucker**[a,b], **Christophe L. M. J. Verlinde**[a,b], **Erkang Fan**[a,b], **Wesley C. Van Voorhis**[a,d], **Frederick S. Buckner**[a,d], **Pradipsinh K. Rathod**[c], **Wim G. J. Hol**[a,b], and **Ethan A. Merritt**[a,b,*]

[a] Medical Structural Genomics of Pathogenic Protozoa Consortium (MSGPP), www.msgpp.org, , University of Washington, Seattle, WA 98195, USA

[b] Department of Biochemistry, University of Washington, Seattle, WA 98195, USA

[c] Department of Chemistry, University of Washington, Seattle, WA 98195, USA

[d] Department of Medicine, University of Washington, Seattle, WA 98195, USA

[e] The Center for High Throughput Structural Biology (CHTSB), Hauptman-Woodward Institute, Buffalo, NY 14203, USA

Abstract

Purine nucleoside phosphorylases and uridine phosphorylases are closely related enzymes involved in purine and pyrimidine salvage, respectively, which catalyze the removal of the ribosyl moiety from nucleosides so that the nucleotide base may be recycled. Parasitic protozoa generally are incapable of *de novo* purine biosynthesis so the purine salvage pathway is of potential therapeutic interest. Information about pyrimidine biosynthesis in these organisms is much more limited. Though all seem to carry at least a subset of enzymes from each pathway, the dependency on *de novo* pyrimidine synthesis versus salvage varies from organism to organism and even from one growth stage to another. We have structurally and biochemically characterized a putative nucleoside phosphorylase from the pathogenic protozoan *Trypanosoma brucei* and find that it is a homodimeric uridine phosphorylase. This is the first characterization of a uridine phosphorylase from a trypanosomal source despite this activity being observed decades ago. Although this gene was broadly annotated as a putative nucleoside phosphorylase, it was widely inferred to be a purine nucleoside phosphorylase. Our characterization of this trypanosomal enzyme shows that it is possible to distinguish between purine and uridine phosphorylase activity at the sequence level based on the absence or presence of a characteristic uridine phosphorylase-specificity insert. We suggest that this recognizable feature may aid in proper annotation of the substrate specificity of enzymes in the nucleoside phosphorylase family.

Keywords

nucleoside phosphorylase; pyrimidine salvage; nucleotide metabolism; sleeping sickness; gene annotation

*Corresponding author. address: merritt@u.washington.edu, Ethan A. Merritt, Department of Biochemistry, Box 357742, University of Washington, Seattle, WA 98195-7742 USA, Phone: (206) 543-1421, Fax: (206) 685-7002.

Introduction

All living cells are dependent on purine and pyrimidine nucleotides to carry out a plethora of biochemical processes. These nucleotides may be synthesized completely *de novo* and/or be salvaged from the cell's environment. Both pathways require multiple enzymes, but the salvage pathway is less costly to the cell energetically. Though many species, including mammals, utilize both *de novo* synthesis and salvage, most parasitic protozoa rely on one pathway or the other to fulfill their purine and pyrimidine requirements.[1; 2; 3] For instance, parasitic protozoa lack *de novo* purine synthesis thus making purine salvage enzymes potentially attractive drug targets. The story for pyrimidine biosynthesis is not as straightforward and, in general, pyrimidine biosynthetic pathways have not been studied to the extent of their purine counterparts amongst parasitic protozoa. Many parasitic protozoa contain at least a subset of the enzymes involved in both *de novo* synthesis and salvage though they may rely more heavily on one pathway versus the other in various life stages to meet their pyrimidine needs.[1; 2; 3; 4] These differing dependencies on *de novo* synthesis or salvage with respect to purines and pyrimidines underscore the importance of correctly annotating the function of the gene products involved in these pathways as they are identified through the various genome projects of protozoan pathogens.

Because of the importance of nucleoside biosynthesis and salvage in protozoa, a putative nucleoside phosphorylase from *Trypanosoma brucei* (GeneDB[5] accession number Tb927.8.4430), the causative agent of African Sleeping Sickness, was selected for investigation as a possible drug target by the Medical Structural Genomics of Pathogenic Protozoa Consortium (www.msgpp.org).[6] Nucleoside phosphorylases are ubiquitous enzymes involved in nucleotide salvage pathways from organisms in all domains of life. They catalyze the reversible cleavage of the glycosidic bond in purine and pyrimidine nucleosides or deoxynucleosides using inorganic phosphate to yield the purine or pyrimidine base and α-ribose-1-phosphate. The free bases can then be used for nucleotide formation *in lieu* of costly *de novo* biosynthesis. The phosphorylase superfamily (Pfam[7] 01048) is subdivided into two families based primarily on structure (reviewed in Pugmire and Ealick, 2002[8]). Each family encompasses many sequences of low identity and a broad substrate range. Members of the nucleoside phosphorylase-I (NP-I) family are single domain proteins that display an α/β-fold and may adopt a hexameric (trimer of dimers) or trimeric quaternary structure. Though there are exceptions, hexameric enzymes are more typical in bacteria while the trimeric enzymes are typically found in mammals. NP-I family members act on a variety of purine or pyrimidine substrates and include purine nucleoside phosphorylase (PNP, EC 2.4.2.1), uridine phosphorylase (UP; EC 2.4.2.3), and 5′-deoxy-5′-methylthioadenosine phosphorylase (EC 2.4.2.28). The NP-I fold is also common to 5′-methylthioadenosine/*S*-adenosylhomocysteine nucleosidase (EC 3.2.2.9) and AMP nucleosidase (EC 3.2.2.4). Nucleoside phosphorylase II (NP-II) family members are two domain proteins with an α/β-fold domain, unrelated to that of the NP-I family, connected to a smaller α-helical domain. NP-II enzymes are specific for pyrimidines, namely uridine and thymidine, and typically function as homodimers.

Though the targeted *T. brucei* gene is annotated generally as a putative nucleoside phosphorylase, it was widely inferred to be a PNP because the majority of proteins returned from a BLAST[9] search are annotated as such. Here we report, however, that close inspection of the results of this search, ignoring sequence annotations of uncharacterized gene products and comparing only to enzymes of characterized activity, suggests it is more similar to UP. Further, when searching the conserved domain database,[10; 11] the sequence returns uridine phosphorylase (COG2820) as the top hit followed by the more broad pfam01048 (PNP_UDP_1, phosphorylase superfamily). But since PNPs and UPs are quite similar in structure and sequence, we did not appreciate this apparently greater similarity to UP in

sequence-based searching until after characterization of the actual activity of the *T. brucei* gene product. Since parasitic protozoa have differing dependencies upon purine and pyrimidine salvage due to differing capacity for *de novo* synthesis of the nucleotides, the true substrate specificity of this putative nucleoside phosphorylase from *T. brucei* is of intrinsic biological and potential therapeutic interest.

To this end, we have solved the crystal structure of a putative nucleoside phosphorylase from the pathogenic protozoa *Trypanosoma brucei* in complex with uracil and α-ribose-1-phosphate, confirming that it is a member of the hexameric family of NP-I nucleoside phosphorylases. Interestingly, the *T. brucei* enzyme is not observed to form the canonical hexameric trimer of dimers characteristic of other family members, but rather exists only as a functional dimer that is stabilized by an intermolecularly coordinated calcium ion. To determine the preferred activity of the enzyme, crystal soaking and cocrystallization experiments as well as activity assays were performed using a series of purine and pyrimidine bases or nucleosides. The results of the activity assays support the crystallographic evidence that this enzyme is a functional uridine phosphorylase. This constitutes the first characterization of a specific trypanosomal uridine phosphorylase despite its activity being suggested in studies of several trypanosomatids decades ago.[12; 13; 14] Further, since the essentiality of this gene product has not been evaluated, we have used RNA interference (RNAi) to determine its potential as an anti-trypanosomal drug target.

Results

Structure of *Trypanosoma brucei* uridine phosphorylase (TbUP)

The x-ray crystallographic structure of the putative nucleoside phosphorylase from *T. brucei*, the causative agent of African sleeping sickness, was solved using multiwavelength anomalous dispersion (MAD) and refined to 1.45 Å resolution (Tables 1 and 2). The asymmetric unit is composed of two copies of the polypeptide that form the biologically relevant homodimer. The final model consists of residue 15 to 341 (the C-terminus of the full length protein) of each monomer, bound uracil and ribose-1-phosphate occupying each active site, an intermolecularly coordinated calcium ion, and 509 water molecules (Figure 1a). The N-terminal His-tag and the first fourteen residues of each monomer are not modeled due to disorder in this region of the proteins.

Each monomer is composed of a central eleven-stranded mixed β-sheet surrounded by fourteen α-helices and two peripheral short, two-stranded anti-parallel β-sheets (Figure 1a). This fold is characteristic of the NP-I family of nucleoside phosphorylases. Indeed, with the exception of a few unusual structural features that will be discussed below, the structure of the TbUP dimer is very similar to that of all other NP-I structures currently available in the Protein Data Bank (PDB[15]), particularly those that utilize (deoxy)uridine as the primary substrate. Two monomers form a tight dimer with approximately 2,765 $Å^2$, just over 18%, of the solvent exposed surface area per monomer buried in the dimer interface as determined by the PISA server.[16] The dimer interface is additionally stabilized by a tightly coordinated metal ion near the center of mass of the molecule (discussed below). The dimer present in the asymmetric unit is equivalent to the dimer unit seen in members of the hexameric NP-I subfamily, however it is not possible to assemble three TbUP dimers into the canonical hexamer, as will be described below. The recent structural characterization of human uridine phosphorylase (hUPP1) has shown that it is also a hexameric NP-I family member that assembles only into a functional dimer[17] but the structural features that prevent hexamer formation are quite different from those of the *T. brucei* enzyme. Because residues from neighboring monomers of the dimer contribute to the active site of NP-I nucleoside phosphorylases, the dimeric assembly of the *T. brucei* and human enzymes constitutes the minimal catalytic unit necessary for activity.

Comparison of the sequence and structure of the *T. brucei* enzyme with other hexameric NP-I family enzymes explains why it does not assemble into the prototypical hexamer. As apparent in a sequence alignment (Figure 1b), the *T. brucei* enzyme contains two large inserts greater than 25 amino acids and two smaller inserts. Two of these inserts create additional secondary structural elements that would protrude into the neighboring dimer of the canonical NP-1 hexamer thus sterically blocking trimerization of the dimers (Figure 1c). The first is a long, largely hydrophilic, helical insert (α6-α7) located immediately upstream of a typically relatively short hydrophobic patch (FPAV in *E. coli* UP) important for the dimer-dimer interaction of the hexamer, which have been replaced by more hydrophilic residues in TbUP (^{199}YTSM^{202}). This region is also responsible for preventing hexamer formation in hUPP1 but the structural details are quite divergent. The human enzyme lacks the large helical insert (Figure 1b) and instead has substituted a short insert and a two-stranded antiparallel β-sheet in the vicinity of TbUP helix α5. It is actually the short insert upstream of this new β-sheet along with the substitution of the typically hydrophobic patch for hydrophilic residues that block hexamer formation of the human enzyme, while the novel β-sheet projects towards the neighboring monomer and effectively increases the buried surface area of the dimer.[17] The second hexamer-blocking insert of TbUP is a short two-stranded antiparallel β-sheet (β11-β12) that lies adjacent to helix α6 (Figure 1c).

Intermolecular metal-binding site

A very strong difference density peak, also corresponding to the largest peak in the anomalous difference Fourier map, was present near the center of mass of the dimer and right between the active site of each monomer (Figures 1a and 1d). This peak was observed in the electron density from all datasets of this protein despite there being no extraneous metals added during expression, purification, or crystallization with the exception of sodium chloride. The site is coordinated by four NCS-related oxygen atoms from each monomer for a total of eight ligands; the carbonyl oxygen of Met^{87}, O$^{\delta 1}$ and O$^{\delta 2}$ of Asp^{90}, and O$^{\delta 1}$ of Asn^{91} from each chain across the NCS two-fold axis. The eight oxygen ligands form a slightly distorted square antiprism around the metal with the bidentate interactions of the two Asp^{90} side chain carboxylates forming one square face and the Met^{87} carbonyl oxygen atoms/Asn91 side chain oxygen atoms forming the other square face (Figure 1d).

This electron density peak was modeled as a calcium ion based on the coordination geometry described above with metal to ligand distances that are characteristic of calcium to oxygen.[18] The assignment of calcium is also supported by the calcium bond-valence sum method (CBVS);[19] a method of using the refined metal to ligand distances and the geometric environment to aid in assignment of appropriate metal ions in crystal structures that is most reliable when the resolution exceeds 1.5Å, which is the case for the TbUP structure. Importantly, the assignment of calcium is supported by CBVS independent of whether the structure is refined with the metal modeled as calcium, potassium, sodium, or zinc, which should have a slight effect on the resulting metal to ligand distances due to the varying restraints on these distances for the different metal ions. The average metal to ligand distance for the final refined calcium ion is 2.5 Å, which is a bit longer than the calcium-donor target distance.[18] However, if each Asp^{90} is treated as a monodentate ligand rather than bidentate by considering only the oxygen of closer proximity to the metal, the average calcium-donor distance is 2.4 Å, which is much closer to the target distance. This still leaves six ligands to the metal in a slightly distorted trigonal prismatic coordination geometry. Both this and the square antiprism coordination geometry described above are consistent with calcium. The final metal to ligand distances are also consistent with those expected for sodium but sodium was rejected as the identity of the metal for two primary reasons. First, there is still a considerable peak in the difference Fourier map after refinement as sodium suggesting that the true metal contains more electrons; and second, a significant peak is present in the anomalous difference

Fourier map and the *f*″ of sodium is essentially zero at the wavelengths used for data collection so an anomalous peak larger than that observed for sulfurs in the structure would not be expected. Since Ca^{2+} was not added in any step of protein production to crystallization, the enzyme likely acquired this metal ion during its bacterial expression.

This is not the first observation of a UP containing an intramolecular metal ion. Some structures of the *E. coli* [20; 21] and the *Salmonella typhimurium*[22] enzymes contain a potassium ion that is situated between active sites in the dimer interface, but not at the structurally equivalent location observed for the calcium ion in the *T. brucei* enzyme. Comparison of structures with and without the potassium ion suggests that the metal plays a structural role, stabilizing tighter dimers within the hexamer that in turn stabilizes the phosphate-binding pockets within the active sites, which accordingly leads to an approximately two-fold enhancement of activity with increasing potassium concentration.[20] It is plausible that TbUP is more dependent on the stabilizing effect of an inter-monomer metal than typical NP-I family nucleoside phosphorylases because it exists only as a dimer rather than the higher order hexameric state, which is suggested to contribute to the overall stability of the enzyme.[22] Along these lines, the human enzyme, hUPP1, also stabilizes its homodimeric structure, but via an alternate strategy. It lacks the residues required for metal coordination (Figure 1b) and rather has greatly increased the size of the dimer interface by reconfiguring the structural elements of the would-be hexamerization interface so that they interact with its monomeric partner instead of another dimer.[17]

Active site pockets and bound products

In common with the dimer unit of all hexameric NP-I family members, the *T. brucei* dimer comes together so that the two active site pockets are approximately 20 Å apart and resemble boots with the toes oriented towards the dimer interface. The catalytically-required phosphate binds in the toe of each boot-shaped active site pocket while the uridine substrate binds with the uracil at the boot's heel and the ribose in the arch region, adjacent to the phosphate (Figure 2a). Most of the amino acids that compose the active site pocket are contributed by a single monomer, but several important residues are contributed by the neighboring monomer including two that make crucial interactions with the substrate/products, namely His^{26} and Arg^{66} (Figures 1b and 2b). The side chain of His^{26} hydrogen bonds with the 5′ hydroxyl of the ribose, while Arg^{66} is a key residue in the phosphate pocket forming two hydrogen bonds with phosphate oxygen atoms. The phosphate is further bound by the nitrogen of Gly^{42} and the side chains of Arg^{46}, Arg^{137} and Thr^{140}. Residues Leu^{25}, His^{26} and Arg^{66} together comprise roughly half of the accessible surface at the opening of the active site pocket. The amino acids responsible for binding the phosphate and ribose moieties of the substrates and products are much more highly conserved between UPs (Figure 2c) and PNPs than are the residues responsible for binding the respective bases (Figures 1b, and 3a). In fact, two of the key UP residues that interact with the uracil, Gln^{246} and Arg^{248} (TbUP numbering), have no analogous amino acids in PNPs and reside on a UP-specific insert. These discriminating residues in conjunction with the insert they are located on may be used to distinguish between the catalytic activities of UP and PNP enzymes at the level of the primary sequence and thus may aid in proper annotation (Figures 1b and 3; discussed below).

In the initial structure that was solved without the addition of organic ligands, phosphate, present in the crystallization solution, was apparent in the phosphate-binding pocket of the active site for each monomer along with an adjacent oddly-shaped but indistinct difference density peak. This peak was located at the position that would be expected for the nucleobase of the substrate or product and was present despite not having added any extraneous potential substrates or products during purification or crystallization of the enzyme. Neither purine nor pyrimidine base could be modeled convincingly into the density and a preference for one class

of base over the other was not clear so we set out to determine enzyme specificity by soaking crystals with or cocrystallizing with various purine and pyrimidine bases and nucleosides. These experiments did not allow this mysterious density to be resolved any more readily than the original structure with the exception of a uridine cocrystal. In this crystal, it was immediately obvious from strong difference density peaks of definable shape in the active site of each monomer that the products of the catalytic reaction, ribose-1-phosphate and free uracil were present (Figure 2b). The phosphate moiety of ribose-1-phosphate is in essentially the identical location as the phosphate observed in the structures that were not cocrystallized with the nucleotide substrate, and clear density for the ribose moiety extends towards the heel of the boot-shaped active site. The ribose is in the C1′-*exo* conformation but the stereochemistry of the anomeric C1′ carbon is opposite what it would be when linked to the nucleobase because of the attack of the phosphate from the opposite face of the sugar ring. The now clear uracil density occupies the approximate location of the previously unfittable density. The active site environment is essentially the same as seen in the product-bound *E. coli* structures (PDB codes 1rxc[20] and 1tgy [Bu, *et al.*, unpublished]) and the inhibitor-bound human UPP1 structure (PDB 3euf[17]), which is not surprising given the high structural and sequence conservation of the active sites (Figure 1b); particularly the residues involved in interactions with the products/substrates (Figure 2c).

When comparing the isomorphous “ligand-free” and ligand-bound structures of TbUP, we do not see the large conformational changes in the active site previously described for the bacterial enzyme.[20] The bacterial structures exhibit a highly flexible “flap” loop that is often disordered and undergoes a large conformational change upon substrate binding.[20] The equivalent TbUP residues, approximately residues ^{312}Val-Gly^{320}, are well-ordered and retain essentially the same conformation in the “ligand-free” and ligand-bound structures. This region of TbUP is slightly longer and conformationally different than that of EcUP and is in a position somewhat intermediate between the open and closed bacterial states. The lack of a conformational change may be because the TbUP “ligand-free” active site is not fully devoid of ligands, as described above, and so we have not captured the true ligand-free conformation. On the other hand, it is also possible that this rigidity is a characteristic of eukaryotic UPs since the equivalent region in hUPP1 remains in essentially the same intermediate conformation between ligand-bound and unbound states.[17]

Enzyme Activity

Since nucleoside phosphorylases that prefer either purine or pyrimidine substrates may still display weak activity against the other, the crystal structure may not be a reliable means of determining specificity. Thus, to identify the actual substrate specificity of TbUP, and to confirm that the preferred substrate is uridine as suggested by the crystallographic experiments, purified enzyme was tested for activity against a series of purine and pyrimidine nucleoside and deoxynucleoside substrates. Among the potential substrates tested for activity, only uridine and deoxyuridine showed detectable cleavage in the presence of the enzyme (Table 3). The strict specificity for pyrimidines by TbUP is in agreement with previous studies of bacterial and mammalian UPs.[8; 23; 24; 25] TbUP does not, however, possess a low activity against thymidine, which is often observed. Also in line with the activity of other UPs, deoxyuridine is a much less efficient substrate of TbUP, being cleaved at a rate only approximately 14% of that seen for uridine. Interestingly, it has been reported for human UP that the activity against deoxyuridine is also about 15% that of uridine.[26] In common with EcUP, three hydrogen bonds are formed with the ribose 2′-hydroxyl group (Figure 2b), providing a likely explanation for the substrate preference of uridine over deoxyuridine.[20] The inability of thymidine to form these hydrogen bonds may contribute to the inability of TbUP to catalyze its phosphorolysis. These biochemical results confirm the crystallographic evidence that TbUP is actually a uridine phosphorylase.

It has been reported that there are two groups of uridine cleaving enzymes distinguished by pH optima; one with an optimum at pH 6.5–6.7 and another with an optimum at pH 7.9–8.1.[23] This prompted us to further test *T. brucei* UP activity for pH dependence using a pH range of 6.0–8.5 (Table 4). Maximal activity with uridine as the substrate is at pH 7.5, which is in agreement with the optimal pH of 7.3 found for activity of EcUP[24]. Curiously, the maximal activity with deoxyuridine as the substrate is much lower at pH 6.5, and the activity against deoxyuridine is much more sensitive to pH change. Approximately 40% decrease in activity is observed on either side of optimum pH when uridine is the substrate but the activity increases about 350% as the pH decreases from 7.5 to 6.5 when deoxyuridine is the substrate. The significance of these observations is not clear, but it is possible that the three hydrogen bonds between the enzyme and the 2′-hydroxyl group and/or the loss of the observed intramolecular hydrogen bond (2.95 Å) between the 2′-hydroxyl and the O1′ of ribose-1-phosphate that would be lost when deoxyuridine is the substrate may play a role in this pH effect.

As mentioned above, maximal activity of bacterial UP is dependent on the presence of an intermolecularly coordinated K^+ ion that stabilizes the active site.[20] To test the possibility that activity of TbUP is likewise influenced by the potentially stabilizing intermolecular Ca^{2+} ion, uridine cleavage was monitored at elevated temperature, 55 °C, in the presence of up to 2 mM EGTA or 0.5 mM $CaCl_2$ (Figure 4). In the presence of EGTA, there is almost a complete loss of activity after about 50 minutes. When the enzyme is supplemented with $CaCl_2$, 60% of the initial activity remains after 90 minutes. In control experiments, when no EGTA or $CaCl_2$ was added, the enzyme loses about 40% of its initial activity after 20 minutes but then only experiences an additional 10% loss over the next 70 minutes. Due to limitations with the experiment, the precise relationship between Ca^{2+} and TbUP activity is not clear, but it is clear that the intermolecularly coordinated metal ion does contribute to the overall stability of the enzyme.

RNA interference of *Trypanosoma brucei* uridine phosphorylase

To evaluate the potential of TbUP as a drug target against *T. brucei*, the gene was subjected to silencing by over-expression of stem-loop RNA from tetracycline-regulated constructs. Messenger RNA levels at 72 hours post-induction were decreased by approximately 90% as measured by quantitative PCR (Figure 5). Bloodstream-form parasite growth for five separate clones was measured over a period of 7 days following induction of RNAi. No growth inhibition was observed over this time period for any of the clones compared to the uninduced controls (Figure 5).

Can UPs and PNPs be annotated correctly from their sequences?

Though annotated with the very broad label, “putative nucleoside phosphorylase,” the Tb927.8.4430 gene product was largely assumed to be a PNP based on BLAST searches and inferred from the links that existed within the gene’s records in GeneDB*, TargetDB, and TDR Targets.[27] As mentioned previously, digging deeper into the sequence comparisons and including consideration for conserved domains seemed to point toward the possibility that the enzyme was really a UP. But, since PNPs and UPs are quite similar in sequence and structure, this marginally greater similarity to UP in sequence-based searching only stood out after the high resolution uridine co-crystal structure had been solved, which suggested UP activity that was later confirmed by biochemical assays. These results then emphasized the existence of a UP-specific insert that was alluded to in early structural studies of EcUP by Morgunova *et al.*[28] and later emphasized by Caradoc-Davies *et al.*[20]

*The gene is now annotated as “uridine phosphorylase, putative” in the current beta version of the next generation of GeneDB (http://beta.genedb.org/NamedFeature?name=Tb927.8.4430).

Realizing that sequence-based searches may have actually been able to correctly identify the activity of the *T. brucei* gene product, we looked at the sequences of homologous proteins from other organisms of interest to the Medical Structural Genomics of Pathogenic Protozoa Consortium (www.msgpp.org) that have not yet been characterized to see if their functions may be clarified. These protein sequences include the "putative nucleoside phosphorylase" in *T. cruzi* (accession numbers XP_814980.1 and XP_811342.1), "nucleoside phosphorylase-like protein" in several species of *Leishmania* (*L. major*: XP_001681435.1; *L. infantum*: XP_001463753.1 and XP_001464547.1; *L. braziliensis*: XP_001562879.1), "purine nucleoside phosphorylase" in *Entamoeba histolytica* (XP_652740.1, XP_654874.1, XP_655398.1), and "UPL-1" in *Giardia lamblia* (XP_001707342.1; this *Giardia* gene product is possibly responsible for the uridine phosphorylase activity previously studied[29; 30]). Indeed, alignment of these sequences with the *T. brucei* gene product characterized herein and other known UPs or PNPs (Figure 3A), shows that all contain the UP-specificity region (amino acids 243-264 in TbUP) that bears the substrate-discriminating glutamine and arginine residues (Gln^{246} and Arg^{248} in TbUP), strongly suggesting that all are *bona fide* UP enzymes. The divergence in UP and PNP sequences in this region leads to differences in structure (Figure 3) that allow for selection of one type of substrate over the other and is suggested to have led to the evolutionary split of hexameric nucleoside phosphorylases with purine or uridine cleavage activity.[20] The presence or absence of this insert may help guide the annotation process. A cursory look at many other nucleoside phosphorylase-like genes obtained in a BLAST search shows that many annotated PNPs are likely to be UPs or *vice versa* and that it may be possible to assign more specific annotation to many that are currently annotated generally as nucleoside phosphorylase.

The alignment additionally suggests that the probable UPs from the MSGPP target organisms, all eukaryotic parasites, likewise function as homodimers (not shown). All of these protozoan gene products have a large insert corresponding to the large hexamer-blocking insert 1 of TbUP. In addition, the other trypanosomatid sequences possess the second, smaller hexamer-blocking insert and the calcium-coordinating motif found in TbUP further supporting a homodimeric quaternary structure. As mentioned previously, human UPP1, the only other eukaryotic UP present in the protein data bank, also is present as a homodimer but has utilized a slightly different, more subtle, structural mechanism to prevent a hexameric quaternary structure and to stabilize the homodimeric form. These features are not as immediately obvious from the sequence alone because there is not a very large hexamer-blocking insert as seen in many protozoan sequences, but the sequence differences are recognizable none-the-less, particularly with the structural context of human UPP1 as a reference. Using this information, it appears that the UPs from many other higher eukaryotes are also dimers. These non-protozoan UP sequences look similar to the dimeric human UPP1 and generally have a small insert and a greater number of hydrophilic residues in the vicinity of the prototypical hexameric dimer-dimer interface.

Discussion

Here we show crystallographically and biochemically that a putative nucleoside phosphorylase from *T. brucei* should be classified more specifically as a uridine phosphorylase (UP, EC 2.4.2.3). The first evidence we saw for uridine cleavage activity of this enzyme was from inspection of a crystal structure following cocrystallization with the substrate uridine in the presence of phosphate buffer. Strong electron density was observed in each active site for the products uracil and ribose-1-phosphate. Although the equivalent complexes with various purines were not obtained despite significant effort, this complex structure alone was not sufficient to assign the function as UP since many PNPs also show low activity against uridine (e.g. the *Plasmodium* PNP[31; 32]). We thus initiated activity assays with purified recombinant enzyme against a panel of pyrimidine and purine (deoxy)nucleosides and found that it is indeed

specific for uracil containing substrates. Interestingly, UP activity shows significant pH dependence with deoxyuridine as the substrate but uridine cleaving activity is not substantially affected in the tested pH range of 6 to 8.5. At pH 7.5, the maximum for uridine cleavage, the activity against uridine is more than five-fold greater than the turnover of deoxyuridine. At pH 6.5, the maximum for deoxyuridine cleavage, the cleavage of uridine is still slightly greater than that of deoxyuridine. This demonstrates that the enzyme has greater specificity for the ribosyl moiety over the deoxyribosyl moiety and is understandable given the hydrogen bonding interaction between the enzyme and the 2′ hydroxyl group of the ribose.

All pyrimidine biosynthesis, whether *de novo* or via salvage, utilizes UMP. Through the salvage pathway, UMP can be formed directly from uridine by the activity of uridine kinase (UK) or indirectly by first being broken down to uracil by either UP or by a nucleoside hydrolase (NH). The uracil is then converted to UMP by uracil phosphoribosyltransferase (UPRT).[3] It is noteworthy that no UK activity has yet been detected in any life stage of any trypanosomatid tested.[12; 33] It thus appears that all UMP formation resulting from the salvage pathway must go through UPRT, the enzyme immediately downstream of UP. As mentioned above, there is potentially overlapping activity between UP and NH, which irreversibly removes the base from the nucleoside using water as the nucleophile, in supplying uracil to UPRT. No specific uridine hydrolases (UH) are known in the trypanosomatids but UH activity has been detected as being distinct from uridine phosphorylase activity in cell extracts of several trypanosomatids.[13] Also, an inosine-uridine preferring nucleoside hydrolase has been characterized in *Crithidia* and *Leishmania*,[34; 35] and there are genes annotated as “putative nucleoside hydrolase” in various trypanosomal genomes. Thus, there may be an alternate means to supply uracil for UPRT on the path to UMP production in these parasites that apparently lack UK activity.[12; 33]

To determine the essentiality of this UP to *T. brucei* in light of its potentially redundant activity, RNA interference experiments were performed on bloodstream-form parasites *in vivo*. UP mRNA levels were knocked down >90%, however no growth effect was observed indicating that the gene function is not essential in this stage of the parasite’s lifecycle, with the caveat that the approximately 5–10% of remaining expression may be sufficient to satisfy the cell requirements. Cellular pools of pyrimidines in *T. brucei* are likely maintained by the combination of *de novo* synthesis and salvage mechanisms.[36] It is also possible that an as-yet uncharacterized NH that is capable of acting on uridine exists in *T. brucei* and is able to compensate for the loss of UP activity. Regardless of the reason, these results suggest that UP is not likely to be a good drug target against *T. brucei*.

The characterization of the true substrate specificity and activity of this *T. brucei* enzyme is still of interest biologically, however, because of the apparent variation in utilization of pyrimidine salvage or *de novo* synthesis in different morphological stages of many trypanosomatids.[3; 37] To the best of our knowledge, this is the first actual characterization of a trypanosomal UP despite uridine cleavage activity being observed in whole cell extracts of blood stage *T. brucei* and in all four major morphological forms of various trypanosomatids over 20 years ago,[12; 13] and suggested from studies over 45 years ago.[14] The newly defined activity of this enzyme warrants further study of its role in pyrimidine salvage and in the balance of uracil and uridine concentrations in the cells of these pathogenic human parasites in their diverse morphological forms and host environments.

Through structural and biochemical studies of EcUP, Caradoc-Davies, *et al.*[20] suggested that the emergence of a UP-specificity region may have given rise to distinct UP and PNP activities from within an equivalent hexameric ancestral structural framework. Indeed, the UP structures from all four species that are currently in the PDB (bacterial: *E. coli* and *S. typhimurium*; eukaryotic: human and the *T. brucei* enzyme described here) contain a homologous sequence insert that exists in a similar structural conformation with the C_α atoms of the key uridine

discriminating residues, Gln^{246} and Arg^{248} (TbUP numbering), superimposing to within 1.5 Å and with similarly oriented side chains. Neither this sequence insert nor the key residues are present in any of the non-uridine specific sequences or structures of NP-I enzymes of characterized activity that we are aware of. We came to appreciate the implication of this observation through the course of this work and applied it to the uncharacterized nucleoside phosphorylase sequences from several other MSGPP target organisms in hopes of gleaning additional insight into their functions. This includes homologous sequences from *T. cruzi* and several species of *Leishmania*, as well as three sequences from *E. histolytica* and one from *Giardia lamblia*. All of these sequences contain the UP-specificity insert and the base-discriminating Gln and Arg residues, leading us to predict that they are likely to possess UP activity. Beyond the sequences of interest to MSGPP, we suggest that the presence or absence of the key uridine-discriminating Gln and Arg amino acids in the context of the UP-specificity region would greatly aid in cleaning up nucleoside phosphorylase gene (mis)annotations that have propagated through sequence databases and in properly annotating current generically annotated nucleoside phosphorylases and new sequences that arise as more and more genomes are sequenced. For example, the PNP sequence from several species of *Plasmodium*, an active antimalarial drug target, is still misannotated as UP in several sequence databases despite an abundance of published research (e.g. [31; 32; 38; 39]) establishing it as a PNP. Even in the absence of this experimental basis, however, it should be possible to correctly annotate these *Plasmodium* gene products as PNP because it is clear from a sequence alignment (Figures 1b and 3a) that it does not possess the UP-specificity region nor the discriminating Gln and Arg residues.

Delving more deeply into the potential evolutionary consequence of the acquisition of the UP-specificity region, it is interesting to note that all UP structures currently available in the PDB are members of the hexameric/dimeric NP-I subfamily while PNP structures are drawn from both hexameric and trimeric subfamilies. This is in agreement with the suggestion that hexameric and trimeric NP-I subfamilies diverged from a common PNP ancestor and then the hexameric subfamily further diverged into bacterial PNPs and UPs.[8] We speculate that it is not coincidental that UPs diverged only from the hexameric subfamily, and that this is a structural correlate of the presence of the sequence insert that confers uridine specificity. The residues responsible for purine base recognition in the PNPs lie in the sequence regions flanking the site of the UP-specificity insert. The conformation of these flanking regions is compatible with both the hexameric and trimeric quaternary assemblies. However, uridine recognition is primarily conferred by Gln^{246} and Arg^{248} displayed by helix α10 of the UP-specificity insert (Figures 1b and 3) and the observed position of the adjacent helix α11 of this insert would sterically block formation of the monomer-monomer interface seen in trimeric PNPs. Thus, the trimeric assembly may have imposed an evolutionary restraint that prevented the acquisition of the insert necessary for recognition of the uridine substrate while the framework of the hexameric/dimeric enzyme, which lacks this structural restraint, was able to diverge into a class with uridine specificity.

In summary, we have structurally and biochemically characterized a putative nucleoside phosphorylase from *T. brucei* and find that it is a uridine phosphorylase with high specificity for uracil-containing (deoxy)nucleosides. Though the structure is very similar to other members of the hexameric NP-I family, it has some unusual features. It is dimeric rather than hexameric, which is the result of several Trypanosome-specific sequence inserts that prevent the dimer-dimer interaction required for hexamerization. Also, it contains an intermolecular calcium ion that helps stabilize the smaller quaternary assembly of TbUP. Comparison of the sequence and structure of TbUP with other UP and PNP NP-I family members has highlighted a UP-specific sequence insert with conserved Gln and Arg amino acids that has two major consequences to the enzyme. It confers the ability to efficiently utilize (deoxy)uridine as a substrate and it appears to be responsible for the observation that UPs belong only to the

hexameric/dimeric NP-I subfamily and not the trimeric NP-I subfamily commonly seen for PNPs among higher Eukaryotes. We suggest that the presence of this distinguishing feature that is identifiable in the primary sequence may aid in proper annotation of the gene products of this important enzyme family.

Materials and Methods

Target cloning, protein expression and purification

The putative nucleoside phosphorylase gene from *T. brucei* (GeneDB[5]: Tb927.8.4430) was selected as a target [TargetDB[40]: Tbru017883AAA] for the Medical Structural Genomics of Pathogenic Protozoa Consortium (MSGPP).[6] The full-length gene was cloned from genomic DNA of *T. brucei* strain TREU927 GUTat 10.1 into the *Escherichia coli* expression vector BG1861, a modified version of pET14b that includes a N-terminal noncleavable hexahistidine tag,[41] using ligation-independent cloning (LIC).[42] Protein was expressed in *Escherichia coli* BL21 [DE3] and purified using immobilized metal affinity chromatography on a Ni-NTA column followed by size exclusion chromatography on a HiLoad Superdex 75 column (Amersham Pharmacia Biotech). Protein was eluted in SGPP buffer (0.5M NaCl, 2mM DTT, 0.025% NaN3, 5% glycerol, 25 mM HEPES at pH 7.5), concentrated to 20 mg/mL, flash frozen in liquid nitrogen, and stored at 80 °C. Selenomethionyl-derivative (SeMet) protein was produced according to the protocols of Studier[43] and SGPP,[44] then purified and stored as described for the native protein except that it was concentrated to 12 mg/ml prior to freezing.

Protein crystallization

Purified native TbUP (20 mg/ml) was screened for crystallization leads at the high-throughput facility at the Hauptman Woodward Institute.[45] Several leads were then optimized in-house using sitting-drop vapor diffusion to produce crystals suitable for data collection. Initial diffraction-quality crystals were grown at 4 °C from a crystallization drop composed of 0.4 μl native protein (20 mg/ml) mixed with 0.4 μl well solution consisting of 39% PEG 8000, 0.1 M NaH_2PO_4, 5 mM DTT, and 0.1 M Tris-HCl pH 8.0). This yielded a crystal that produced a poor quality data set from which we were unable to solve the structure by molecular replacement. Assuming that this was due to the low sequence identity (near 25%) with the closest available structure, crystallization of SeMet protein was pursued. Diffraction-quality SeMet crystals were obtained by setting up a fine screen of pH versus [PEG 8000] around the initial condition both with and without the DTT additive using protein at 12 mg/ml. Most drops immediately precipitated while setting up this screen, so it was repeated with the addition of an equal amount of Milli-Q H_2O to the drop, thereby decreasing the initial concentrations of all components by one-third. This produced Se-Met crystals suitable for data collection. The mother liquor of the crystal that led to the initial phases was 37% PEG 8000, 0.1 M NaH_2PO_4, 0.1 M Tris-HCl (pH 7.9). No cryoprotectant was necessary, so crystals were mounted in cryoloops and directly frozen in liquid nitrogen in preparation for diffraction experiments.

To shed light on the substrate specificity of the enzyme, crystals of native and SeMet crystals were soaked with various purine and pyrimidine nucleosides, deoxynucleosides, and bases. Soaking experiments were performed with substrate concentrations varying from 10 to 33 mM and for times ranging from 1 to 72 hours. Soaking failed to yield an interpretable complex structure so we turned to cocrystallization. Cocrystallization experiments were set up as described above for SeMet protein, except that both native and SeMet protein (each diluted to 10 mg/ml with SGPP buffer) were used and an equal volume of 10 mM nucleoside, deoxynucleoside, or base was added to the drop rather than water. Only native protein was used to further optimize cocrystals. Cocrystals of the phosphorylase: uridine structure described herein grew from an initial mixture of 1 μl native protein solution (15 mg/ml) + 1

μl 10 mM uridine + 1 μl well solution [39 % PEG 8000, 0.1 M unbuffered NaH_2PO_4, 0.1 M Tris-HCL (pH 8.5)] equilibrated over 80 μl well solution at 4 °C.

Data collection and structure determination

Crystals of TbUP were screened at the Stanford Synchrotron Research Lightsource (SSRL) on beamline 9-2 using the SSRL automated mounting (SAM) system.[46] Data were collected at 100 K on a MarMosaic-325 CCD detector using the Blu-Ice software package.[47] Multiwavelength anomalous dispersion (MAD) data were collected at the Se peak and remote wavelengths, as determined from a fluorescence scan of a single crystal of SeMet protein. 160° of data with 1° oscillation/image were collected at the Se-peak wavelength but only 80° of data were collected at the remote wavelength due to crystal decay. 180° of single wavelength data were collected from crystals or cocrystals of native protein. All data were processed using HKL2000.[48] The crystals belong to space group $P2_1$ with unit cell dimensions of approximately 63.1 Å × 95.5 Å × 63.5 Å and a β angle of 105.9°. The Matthews coefficient[49] is approximately 2.4 $Å^3$/Da with two protein molecules, forming a homodimer, present in the asymmetric unit. Data in the highest resolution shell of the uridine cocrystal suffered from high mosaicity, leading to many overlapping reflections in some portions of reciprocal space. Data collection statistics are presented in Table 1.

Using the two-wavelength MAD dataset, SOLVE[50] found 22 Se sites out of 26 expected and produced initial phases to 2.3 Å. Of the sites identified, eighteen subsequently proved to be true selenium sites, one was a metal ion, and three were questionable. The remote wavelength data was included in the initial phase determination steps to help break the ambiguity despite the low completeness and no subsequent effort was made to solve the phase problem via single wavelength anomalous dispersion (SAD) since MAD was successful. The results from SOLVE were then fed into RESOLVE[50] for density modification and automated model building. RESOLVE identified the two-fold noncrystallographic symmetry (NCS) from the heavy atom positions and was able to build 571 residues, placing 554 side chains, out of 698 residues expected for two copies of the full length construct. Iterated manual model building and restrained refinement continued using the Se-peak dataset with Coot[51] and REFMAC5.[52]

When higher resolution data (1.45 Å) were later obtained from a crystal of native protein cocrystallized with uridine, subsequent cycles of building and refinement used this dataset. Based on the difference density present in the active site of the cocrystal structure, it was immediately clear that the enzyme had converted the uridine to the products uracil and ribose-1-phosphate. Ideal coordinates for these products were obtained from the HIC-Up database[53] and they were placed into the difference density peaks using Coot. Refinement restraints for use in REFMAC5 and Coot were obtained from the PRODRG server.[54] In the final cycles of refinement, perturbational displacement of the protein was described by eleven TLS groups per chain as identified by the TLSMD server[55; 56] and TLS parameters were refined for each group prior to restrained refinement in REFMAC5. Model quality was monitored and validated using Coot and MolProbity.[57] The CCP4 suite of programs[58; 59] was used extensively for all steps from data preparation through refinement. Model refinement statistics are presented in Table 2. Molecular figures were created and rendered with PyMOL.[60]

Accession Numbers

Atomic coordinates and structure factors for TbUP have been deposited in the Protein Data Bank[15] (http://www.pdb.org) with accession number 3BJE.

Assays of catalytic activity

To determine the substrate specificity of TbUP, purified protein was tested for activity against different purine and pyrimidine nucleoside and deoxynucleoside substrates as described below.

All enzymatic assays were carried out in assay buffer [50 mM potassium phosphate buffer (pH 7.5) containing 5% glycerol and 2mM DTT] at a protein concentration of 2 μg/ml (determined by Bradford assay). Control experiments were carried out in the absence of either enzyme or substrate in the assay mixture, unless specified. All assays were performed at 25 °C using a Beckman DU 530 UV/visible spectrophotometer.

Inosine as substrate: A coupled enzymatic assay was used to monitor the hydrolysis of inosine to hypoxanthine.[32] Subsequent oxidation of the product hypoxanthine into uric acid by xanthine oxidase was monitored at 293 nm (E_{293} = 12.9 mM^{-1} cm^{-1}). Inosine was used at 0.2 mM.

Guanosine/deoxyguanosine as substrate: Hydrolysis of guanosine/deoxyguanosine was monitored directly at 262.5 nm ($E_{262.5}$ = −3.6 mM^{-1} cm^{-1}).[61] Guanosine/deoxyguanosine was used at 0.2 mM.

Adenosine/deoxyadenosine as substrate: Two methods were used. **1)** Hydrolysis of adenosine/deoxyadenosine was monitored directly at 274 nm (E_{274} = −1.9 mM^{-1} cm^{-1}).[38] Adenosine/deoxyadenosine was used at 0.2 mM. **2)** A coupled enzymatic assay was used to monitor the reverse reaction, synthesis of adenosine from D-(3′-deoxy)ribose-1-phosphate and adenine. Subsequent deamination of the product adenosine by adenosine deaminase was monitored at 265 nm (E_{265} = −6.4 mM^{-1} cm^{-1}).[62] Adenine and D-ribose1-phosphate were used at 80 and 240 μM, respectively.

Uridine/deoxyuridine as substrate: Hydrolysis of uridine/deoxyuridine was monitored directly at 282 nm (E_{282} = −1.37 mM^{-1} cm^{-1}).[63] The reaction requires inorganic phosphate so 50 mM Tris-HCl, pH 7.5 buffer was substituted for the phosphate buffer in the reaction mixture as a control. Uridine/deoxyuridine was used at 0.4 mM.

Thymidine as substrate: Hydrolysis of thymidine was monitored directly at 290 nm (E_{290} = −1.0 mM^{-1} cm^{-1}).[63] Thymidine was used at 1.0 mM.

Cytidine/deoxycytidine as substrate: Hydrolysis of cytidine/deoxycytidine was monitored directly at 270 nm (E_{270} = −3.0 mM^{-1} cm^{-1}).[62] Cytidine/deoxycytidine was used at 0.2 mM.

Effect of pH on UP activity: The reaction was essentially performed and monitored as described above for uridine/deoxyuridine as substrate but was carried out in 50 mM phosphate buffer containing 5% glycerol and 2 mM DTT at pH range of 6.0–8.5.

Effect of calcium on UP activity/stability: thermal inactivation studies were carried out in the [64] presence of EGTA or $CaCl_2$ similarly to those previously published for calcium-dependent peroxidase. For each reaction, 200 μg/ml of enzyme in 50mM phosphate buffer (pH 7.5) containing 1 mM DTT was incubated at 55 °C in the presence of 0, 1, or 2 mM EGTA or 0.5 mM $CaCl_2$. The control reaction did not contain EGTA or $CaCl_2$. At various time intervals, a 5 μl sample was drawn from the reaction mixture and uridine hydrolysis activity was monitored as described above except that the reaction buffer additionally contained EGTA or $CaCl_2$ if needed. No difference in activity was observed for 1 or 2 mM EGTA and it was not possible to raise the $CaCl_2$ concentration above 0.5 mM because of severe interference with spectrophotometric readings as time progressed.

RNAi knockdown of *Trypanosoma brucei* uridine phosphorylase gene product

A region of the TbUP gene sequence (Tb927.8.4430) was selected for RNAi using the program RNAit.[65] Bases 599–910 of the gene were amplified from *T. brucei* 927 genomic DNA using the primers 5′-ATACCAATGTGATGGCATCAATGGCGCATCCCAATA-3′ and 5′-

ATACCATAGAGTTGGCGGCTCCAGCTTGATAACC-3′. The amplicon was ligated using TA cloning into the vector pGEM-T (Promega, cat #A3600), then excised with the enzyme BstXI. This insert was ligated into the stem-loop RNAi vector, pQuadra3, as previously described.[66] The construct was sequenced to verify the identity of the insert and then linearized with NotI in preparation for electroporation. *Trypanosoma brucei* bloodstream-form parasites expressing the T7 RNA polymerase and the Tet repressor under a single selection marker were provided by G. Cross (Rockefeller University).[67] Electroporation and culture methods were done as previously described.[36] Individual clones were selected for subsequent RNAi studies. The expression of the stem-loop RNA was induced by addition of 1 μg/ml tetracycline to the cultures diluted to 1×10^5 cells/ml. Cultures were passed at a 1:10–1:20 dilution daily and cell concentrations were monitored using an ATPLite Luminescence ATP detection Assay System (PerkinElmer, cat#6016941). cDNA was prepared from messenger RNA collected 72 h post-RNAi induction with tetracycline. mRNA signal knock-down was analyzed by quantitative PCR of the cDNA using primers 5′-ATGGCTGCATCCGCTAATGG-3′ and 5′-GGGGAACCGACTCAGCAGG-3′, which amplified a separate region of the gene than that which was used for the RNAi construct. The amplified products from different PCR cycles were quantified by densitometry (normalized to beta-tubulin).

Acknowledgments

We thank Isolde Le Trong for assistance with crystal screening, Christine Stewart for bioinformatics and database expertise, and the rest of the MSGPP team for exceptional support and fruitful discussions. Financial support from the Protein Structure Initiative award NIGMS GM64655 and from NIAID award AI067921 is gratefully acknowledged. Portions of this research were carried out at the Stanford Synchrotron Radiation Lightsource (SSRL), a national user facility operated by Stanford University on behalf of the U.S. Department of Energy, Office of Basic Energy Sciences. The SSRL Structural Molecular Biology Program is supported by the Department of Energy, Office of Biological and Environmental Research and by the National Institutes of Health, National Center for Research Resources, Biomedical Technology Program, and the National Institute of General Medical Sciences.

Abbreviations

Tb	*Trypanosoma brucei*
UP	uridine phosphorylase
PNP	purine nucleoside phosphorylase
NP	nucleoside phosphorylase
RNAi	RNA interference
MAD	multiwavelength anomalous dispersion
hUPP1	human uridine phosphorylase 1
PDB	Protein Data Bank
NH	nucleoside hydrolase
UPRT	uracil phosphoribosyltransferase
UK	uridine kinase
UH	uridine hydrolase
SeMet	selenomethionine
NCS	noncrystallographic symmetry

References

1. Berens, RL.; Krug, EC.; Marr, JJ. Purine and Pyrimidine Metabolism. In: Marr, JJ.; Muller, M., editors. Biochemistry and Molecular Biology of Parasites. Academic Press Limited; London: 1995.
2. Carter, NS.; Rager, N.; Ullman, B. Purine and pyrimidine transport and metabolism. In: Marr, JJ.; Nilson, TW.; Komuniecki, RW., editors. Molecular Medical Parasitology. Academic Press; London: 2002.
3. Hammond DJ, Gutteridge WE. Purine and pyrimidine metabolism in the trypanosomatidae. Mol Biochem Parasitol 1984;13:243–261. [PubMed: 6396514]
4. Gudin S, Quashie NB, Candlish D, Al-Salabi MI, Jarvis SM, Ranford-Cartwright LC, de Koning HP. Trypanosoma brucei: A survey of pyrimidine transport activities. Exp Parasitol 2006;114:118–125. [PubMed: 16620810]
5. Hertz-Fowler C, Peacock CS, Wood V, Aslett M, Kerhornou A, Mooney P, Tivey A, Berriman M, Hall N, Rutherford K, Parkhill J, Ivens AC, Rajandream MA, Barrell B. GeneDB: a resource for prokaryotic and eukaryotic organisms. Nucleic Acids Res 2004;32:D339–343. [PubMed: 14681429]
6. Fan, E.; Baker, D.; Gelb, MH.; Buckner, FS.; Van Voorhis, WC.; Phizicky, E.; Dumont, M.; Mehlin, C.; Grayhack, EJ.; Sullivan, M.; Verlinde, CL.; DeTitta, G.; Meldrum, D.; Merritt, EA.; Earnest, TN.; Soltis, M.; Zucker, F.; Myler, P.; Schoenfeld, L.; Kim, D.; Worthey, EA.; LaCount, D.; Vignali, M.; Li, J.; Mondal, S.; Massey, A.; Carroll, B.; Gulde, S.; Luft, JR.; DeSoto, L.; Holl, M.; Caruthers, JM.; Bosch, J.; Robien, MA.; Arakaki, T.; Holmes, MA.; Le Trong, I.; Hol, WG. Structural Genomics of Pathogenic Protozoa: An Overview. In: Bostjan, K.; Mitchell, G.; Huber, T., editors. Methods Mol Biol. Vol. 426. 2008. p. 497-513.
7. Finn RD, Tate J, Mistry J, Coggill PC, Sammut SJ, Hotz HR, Ceric G, Forslund K, Eddy SR, Sonnhammer ELL, Bateman A. The Pfam protein families database. Nucleic Acids Res 2008;36:D281–288. [PubMed: 18039703]
8. Pugmire MJ, Ealick SE. Structural analyses reveal two distinct families of nucleoside phosphorylases. Biochem J 2002;361:1–25. [PubMed: 11743878]
9. Altschul SF, Madden TL, Schäffer AA, Zhang J, Zhang Z, Miller W, Lipman DJ. Gapped BLAST and PSI-BLAST: a new generation of protein database search programs. Nucleic Acids Res 1997;25:3389–3402. [PubMed: 9254694]
10. Geer LY, Domrachev M, Lipman DJ, Bryant SH. CDART: Protein Homology by Domain Architecture. Genome Res 2002;12:1619–1623. [PubMed: 12368255]
11. Marchler-Bauer A, Anderson JB, Derbyshire MK, DeWeese-Scott C, Gonzales NR, Gwadz M, Hao L, He S, Hurwitz DI, Jackson JD, Ke Z, Krylov D, Lanczycki CJ, Liebert CA, Liu C, Lu F, Lu S, Marchler GH, Mullokandov M, Song JS, Thanki N, Yamashita RA, Yin JJ, Zhang D, Bryant SH. CDD: a conserved domain database for interactive domain family analysis. Nucleic Acids Res 2007;35:D237–240. [PubMed: 17135202]
12. Hammond DJ, Gutteridge WE. UMP synthesis in the kinetoplastida. Biochim Biophys Acta 1982;718:1–10. [PubMed: 6753942]
13. Hassan HF, Coombs GH. A comparative study of the purine- and pyrimidine-metabolising enzymes of a range of trypanosomatids. Comp Biochem Physiol B: Biochem Mol Biol 1986;84:217–223.
14. Jaffe JJ. The effect of 6-Azauracil upon Trypanosoma equiperdum. Biochem Pharmacol 1961;8:216–223. [PubMed: 14450868]
15. Berman HM, Westbrook J, Feng Z, Gilliland G, Bhat TN, Weissig H, Shindyalov IN, Bourne PE. The Protein Data Bank. Nucleic Acids Res 2000;28:235–242. [PubMed: 10592235]
16. Krissinel E, Henrick K. Inference of Macromolecular Assemblies from Crystalline State. J Mol Biol 2007;372:774–797. [PubMed: 17681537]
17. Roosild T, Castronovo S, Fabbiani M, Pizzorno G. Implications of the structure of human uridine phosphorylase 1 on the development of novel inhibitors for improving the therapeutic window of fluoropyrimidine chemotherapy. BMC Struct Biol 2009;9:14. [PubMed: 19291308]
18. Harding M. Small revisions to predicted distances around metal sites in proteins. Acta Crystallogr, Sect D: Biol Crystallogr 2006;62:678–682. [PubMed: 16699196]
19. Muller P, Kopke S, Sheldrick GM. Is the bond-valence method able to identify metal atoms in protein structures? Acta Crystallogr, Sect D: Biol Crystallogr 2003;59:32–37. [PubMed: 12499536]

20. Caradoc-Davies TT, Cutfield SM, Lamont IL, Cutfield JF. Crystal structures of *Escherichia coli* uridine phosphorylase in two native and three complexed forms reveal basis of substrate specificity, induced conformational changes and influence of potassium. J Mol Biol 2004;337:337–354. [PubMed: 15003451]
21. Bu W, Settembre EC, el Kouni MH, Ealick SE. Structural basis for inhibition of Escherichia coli uridine phosphorylase by 5-substituted acyclouridines. Acta Crystallogr, Sect D: Biol Crystallogr 2005;61:863–872. [PubMed: 15983408]
22. Lashkov A, Zhukhlistova N, Gabdulkhakov A, Mikhailov A. Comparative analysis of three-dimensional structures of homodimers of uridine phosphorylase from Salmonella typhimurium in the unligated state and in a complex with potassium ion. Crystallogr Rep 2009;54:267–278.
23. Krenitsky TA, Mellors JW, Barclay RK. Pyrimidine Nucleosidases. Their classification and relationship to uric acid ribonucleoside phosphorylase. J Biol Chem 1965;240:1281–1286. [PubMed: 14284737]
24. Leer JC, Hammer-Jespersen K, Schwartz M. Uridine Phosphorylase from *Escherichia coli*. Eur J Biochem 1977;75:217–224. [PubMed: 16751]
25. Vita A, Amici A, Cacciamani T, Lanciotti M, Magni G. Uridine phosphorylase from Escherichia coli B. enzymatic and molecular properties. Int J Biochem 1986;18:431–435. [PubMed: 3519310]
26. Liu M, Cao D, Russell R, Handschumacher RE, Pizzorno G. Expression, Characterization, and Detection of Human Uridine Phosphorylase and Identification of Variant Uridine Phosphorolytic Activity in Selected Human Tumors. Cancer Res 1998;58:5418–5424. [PubMed: 9850074]
27. Aguero F, Al-Lazikani B, Aslett M, Berriman M, Buckner FS, Campbell RK, Carmona S, Carruthers IM, Chan AWE, Chen F, Crowther GJ, Doyle MA, Hertz-Fowler C, Hopkins AL, McAllister G, Nwaka S, Overington JP, Pain A, Paolini GV, Pieper U, Ralph SA, Riechers A, Roos DS, Sali A, Shanmugam D, Suzuki T, Van Voorhis WC, Verlinde CLMJ. Genomic-scale prioritization of drug targets: the TDR Targets database. Nat Rev Drug Discovery 2008;7:900–907.
28. Morgunova EY, Mikhailov AM, Popov AN, Blagova EV, Smirnova EA, Vainshtein BK, Mao C, Armstrong SR, Ealick SE, Komissarov AA, Linkova EV, Burlakova AA, Mironov AS, Debabov VG. Atomic structure at 2.5 A resolution of uridine phosphorylase from E. coli as refined in the monoclinic crystal lattice. FEBS Lett 1995;367:183–187. [PubMed: 7796917]
29. Jiménez BM, Kranz P, Lee CS, Gero AM, O'Sullivan WJ. Inhibition of uridine phosphorylase from Giardia lamblia by pyrimidine analogs. Biochem Pharmacol 1989;38:3785–3789. [PubMed: 2597172]
30. Lee CS, Jimenez BM, O'Sullivan WJ. Purification and characterization of uridine (thymidine) phosphorylase from Giardia lamblia. Mol Biochem Parasitol 1988;30:271–277. [PubMed: 3185613]
31. Kicska GA, Tyler PC, Evans GB, Furneaux RH, Kim K, Schramm VL. Transition State Analogue Inhibitors of Purine Nucleoside Phosphorylase from Plasmodium falciparum. J Biol Chem 2002;277:3219–3225. [PubMed: 11707439]
32. Schnick C, Robien MA, Brzozowski AM, Dodson EJ, Murshudov GN, Anderson L, Luft JR, Mehlin C, Hol WGJ, Brannigan JA, Wilkinson AJ. Structures of Plasmodium falciparum purine nucleoside phosphorylase complexed with sulfate and its natural substrate inosine. Acta Crystallogr, Sect D: Biol Crystallogr 2005;61:1245–1254. [PubMed: 16131758]
33. Carter NS, Yates P, Arendt CS, Boitz JM, Ullman B. Purine and pyrimidine metabolism in *Leishmania*. Adv Exp Med Biol 2008;625:141–154. [PubMed: 18365665]
34. Parkin DW, Horenstein BA, Abdulah DR, Estupinan B, Schramm VL. Nucleoside hydrolase from Crithidia fasciculata. Metabolic role, purification, specificity, and kinetic mechanism. J Biol Chem 1991;266:20658–20665. [PubMed: 1939115]
35. Shi W, Schramm VL, Almo SC. Nucleoside Hydrolase from Leishmania major. Cloning, expression, catalytic properties, transition state inhibitors, and the 2.5-angstrom crystal structure. J Biol Chem 1999;274:21114–21120. [PubMed: 10409664]
36. Arakaki TL, Buckner FS, Gillespie JR, Malmquist NA, Phillips MA, Kalyuzhniy O, Luft JR, DeTitta GT, Verlinde CLMJ, Van Voorhis WC, Hol WGJ, Merritt EA. Characterization of *Trypanosoma brucei* dihydroorotate dehydrogenase as a possible drug target; structural, kinetic and RNAi studies. Mol Microbiol 2008;68:37–50. [PubMed: 18312275]

37. Gutteridge WE, Gaborak M. A re-examination of purine and pyrimidine synthesis in the three main forms of Trypanosoma cruzi. Int J Biochem 1979;10:415–422. [PubMed: 383542]
38. Chaudhary K, Ting LM, Kim K, Roos DS. *Toxoplasma gondii* purine nucleoside phosphorylase biochemical characterization, inhibitor Profiles, and comparison with the *Plasmodium falciparum* ortholog. J Biol Chem 2006;281:25652–25658. [PubMed: 16829527]
39. Madrid DC, Ting LM, Waller KL, Schramm VL, Kim K. Plasmodium falciparum Purine Nucleoside Phosphorylase Is Critical for Viability of Malaria Parasites. J Biol Chem 2008;283:35899–35907. [PubMed: 18957439]
40. Chen L, Oughtred R, Berman HM, Westbrook J. TargetDB: a target registration database for structural genomics projects. Bioinformatics 2004;20:2860–2862. [PubMed: 15130928]
41. Alexandrov A, Vignali M, LaCount DJ, Quartley E, de Vries C, De Rosa D, Babulski J, Mitchell SF, Schoenfeld LW, Fields S, Hol WG, Dumont ME, Phizicky EM, Grayhack EJ. A Facile Method for High-throughput Co-expression of Protein Pairs. Mol Cell Proteomics 2004;3:934–938. [PubMed: 15240823]
42. Aslanidis C, de Jong PJ. Ligation-independent cloning of PCR products (LIC-PCR). Nucleic Acids Res 1990;18:6069–6074. [PubMed: 2235490]
43. Studier FW. Protein production by auto-induction in high-density shaking cultures. Protein Expression Purif 2005;41:207–234.
44. Mehlin C, Boni E, Buckner FS, Engel L, Feist T, Gelb MH, Haji L, Kim D, Liu C, Mueller N, Myler PJ, Reddy JT, Sampson JN, Subramanian E, Van Voorhis WC, Worthey E, Zucker F, Hol WGJ. Heterologous expression of proteins from Plasmodium falciparum: Results from 1000 genes. Mol Biochem Parasitol 2006;148:144–160. [PubMed: 16644028]
45. Luft JR, Collins RJ, Fehrman NA, Lauricella AM, Veatch CK, DeTitta GT. A deliberate approach to screening for initial crystallization conditions of biological macromolecules. J Struct Biol 2003;142:170–179. [PubMed: 12718929]
46. Cohen AE, Ellis PJ, Miller MD, Deacon AM, Phizackerley RP. An automated system to mount cryo-cooled protein crystals on a synchrotron beamline, using compact sample cassettes and a small-scale robot. J Appl Crystallogr 2002;35:720–726.
47. McPhillips TM, McPhillips SE, Chiu HJ, Cohen AE, Deacon AM, Ellis PJ, Garman E, Gonzalez A, Sauter NK, Phizackerley RP, Soltis SM, Kuhn P. Blu-Ice and the Distributed Control System: software for data acquisition and instrument control at macromolecular crystallography beamlines. J Synchrotron Radiat 2002;9:401–406. [PubMed: 12409628]
48. Otwinowski Z, Minor W. Processing of X-ray diffraction data collected in oscillation mode. Methods Enzymol 1997;276:307–326.
49. Matthews BW. Solvent content of protein crystals. J Mol Biol 1968;33:491–497. [PubMed: 5700707]
50. Terwilliger T. SOLVE and RESOLVE: automated structure solution, density modification and model building. J Synchrotron Radiat 2004;11:49–52. [PubMed: 14646132]
51. Emsley P, Cowtan K. Coot: model-building tools for molecular graphics. Acta Crystallogr, Sect D: Biol Crystallogr 2004;60:2126–2132. [PubMed: 15572765]
52. Murshudov GN, Vagin AA, Dodson EJ. Refinement of macromolecular structures by the maximum-likelihood method. Acta Crystallogr, Sect D: Biol Crystallogr 1997;53:240–255. [PubMed: 15299926]
53. Kleywegt G. Crystallographic refinement of ligand complexes. Acta Crystallogr, Sect D: Biol Crystallogr 2007;63:94–100. [PubMed: 17164531]
54. Schuttelkopf AW, van Aalten DMF. PRODRG: a tool for high-throughput crystallography of protein-ligand complexes. Acta Crystallogr, Sect D: Biol Crystallogr 2004;60:1355–1363. [PubMed: 15272157]
55. Painter J, Merritt EA. TLSMD web server for the generation of multi-group TLS models. J Appl Crystallogr 2006;39:109–111.
56. Painter J, Merritt EA. Optimal description of a protein structure in terms of multiple groups undergoing TLS motion. Acta Crystallogr, Sect D: Biol Crystallogr 2006;62:439–450. [PubMed: 16552146]
57. Davis IW, Leaver-Fay A, Chen VB, Block JN, Kapral GJ, Wang X, Murray LW, Arendall WB III, Snoeyink J, Richardson JS, Richardson DC. MolProbity: all-atom contacts and structure validation for proteins and nucleic acids. Nucleic Acids Res 2007;35:W375–383. [PubMed: 17452350]

58. Collaborative Computational Project Number 4. The CCP4 suite: programs for protein crystallography. Acta Crystallogr, Sect D: Biol Crystallogr 1994;50:760–763. [PubMed: 15299374]
59. Potterton E, Briggs P, Turkenburg M, Dodson E. A graphical user interface to the CCP4 program suite. Acta Crystallogr, Sect D: Biol Crystallogr 2003;59:1131–1137. [PubMed: 12832755]
60. DeLano, WL. The PyMOL Molecular Graphics System. 2002. http://www.pymol.org
61. Koszalka GW, Vanhooke J, Short SA, Hall WW. Purification and properties of inosine-guanosine phosphorylase from Escherichia coli K-12. J Bacteriol 1988;170:3493–3498. [PubMed: 3042752]
62. Hansen MR, Dandanell G. Purification and characterization of RihC, a xanthosine-inosine-uridine-adenosine-preferring hydrolase from Salmonella enterica serovar Typhimurium. Biochim Biophys Acta 2005;1723:55–62. [PubMed: 15784179]
63. Krenitsky TA, Tuttle JV, Koszalka GW, Chen IS, Beacham LM 3rd, Rideout JL, Elion GB. Deoxycytidine kinase from calf thymus. Substrate and inhibitor specificity. J Biol Chem 1976;251:4055–4061. [PubMed: 932021]
64. Mura A, Longu S, Padiglia A, Rinaldi AC, Floris G, Medda R. Reversible thermal inactivation and conformational states in denaturant guanidinium of a calcium-dependent peroxidase from Euphorbia characias. International Journal of Biological Macromolecules 2005;37:205–211. [PubMed: 16336996]
65. Redmond S, Vadivelu J, Field MC. RNAit: an automated web-based tool for the selection of RNAi targets in Trypanosoma brucei. Mol Biochem Parasitol 2003;128:115–118. [PubMed: 12706807]
66. Inoue M, Nakamura Y, Yasuda K, Yasaka N, Hara T, Schnaufer A, Stuart K, Fukuma T. The 14–3-3 Proteins of Trypanosoma brucei Function in Motility, Cytokinesis, and Cell Cycle. J Biol Chem 2005;280:14085–14096. [PubMed: 15653691]
67. Wirtz E, Leal S, Ochatt C, Cross GAM. A tightly regulated inducible expression system for conditional gene knock-outs and dominant-negative genetics in Trypanosoma brucei. Mol Biochem Parasitol 1999;99:89–101. [PubMed: 10215027]
68. Armougom F, Moretti S, Poirot O, Audic S, Dumas P, Schaeli B, Keduas V, Notredame C. Expresso: automatic incorporation of structural information in multiple sequence alignments using 3D-Coffee. Nucleic Acids Res 2006;34:W604–608. [PubMed: 16845081]
69. Beitz E. TeXshade: shading and labeling of multiple sequence alignments using LaTeX2e. Bioinformatics 2000;16:135–139. [PubMed: 10842735]
70. Read R. Improved Fourier coefficients for maps using phases from partial structures with errors. Acta Crystallogr, Sect A: Found Crystallogr 1986;42:140–149.
71. Krissinel E, Henrick K. Secondary-structure matching (SSM), a new tool for fast protein structure alignment in three dimensions. Acta Crystallogr, Sect D: Biol Crystallogr 2004;60:2256–2268. [PubMed: 15572779]

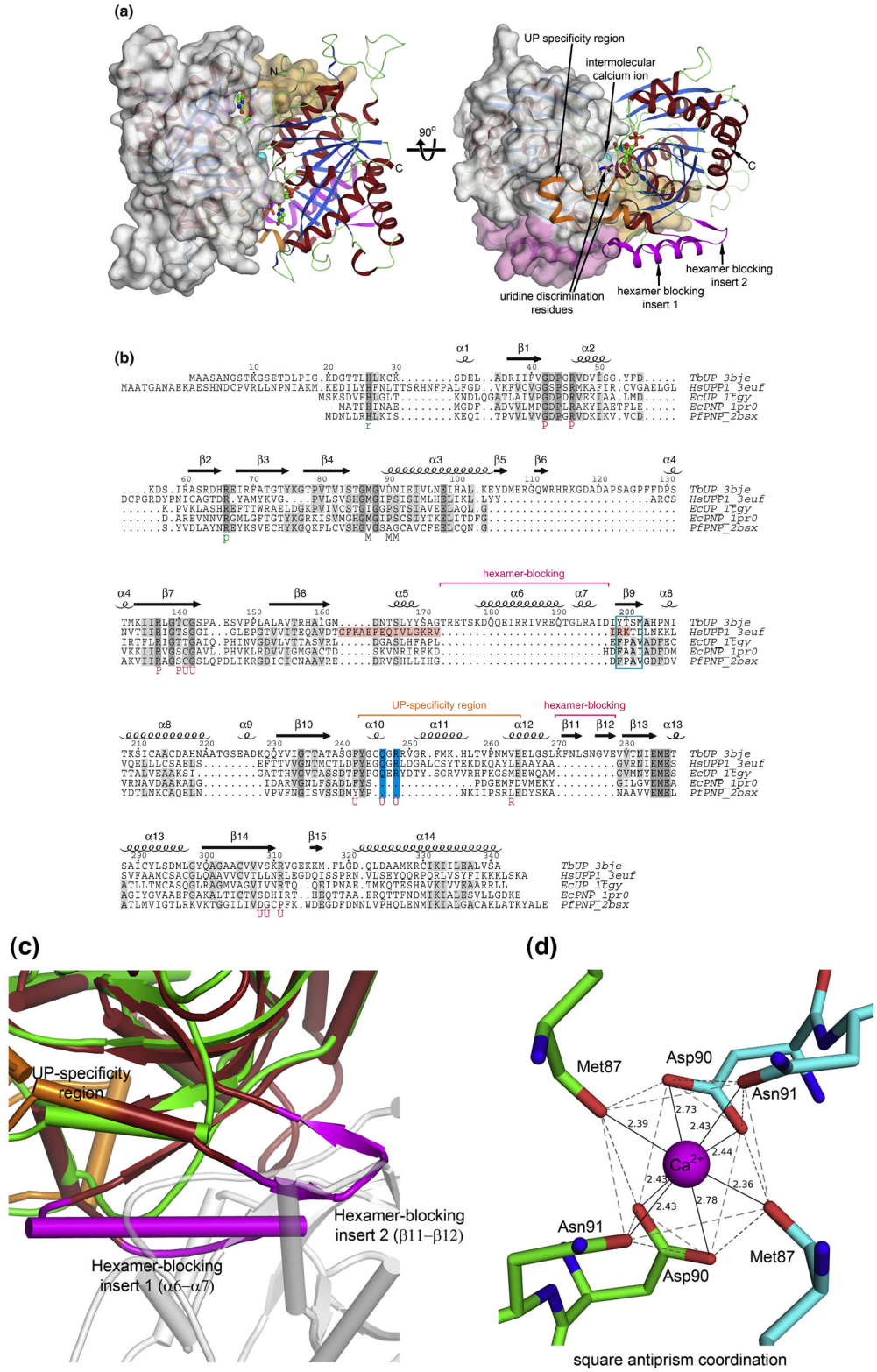

Figure 1.

Structure of homodimeric uridine phosphorylase from *T. brucei*. **(a)** One monomer is shown as a semitransparent white surface with the UP-specificity region orange and the hexamer-blocking inserts magenta. The other monomer is a ribbon diagram with α-helices colored red, β-strands colored blue and loops colored green with the exception of the UP-specificity region and the hexamer-blocking inserts, which are colored orange and magenta, respectively as for the surface monomer. Uracil and α-ribose-1-phosphate products highlight the active sites and are shown as ball-and-sticks. The intermolecular calcium ion is shown as a sphere. The view for the left-hand panel is into the active sites down the two-fold axis and the right-hand panel has been rotated 90° along the depicted axis. **(b)** Structure-based sequence alignment of representative uridine phosphorylases and purine nucleoside phosphorylases. Amino acid numbering and secondary structural elements of TbUP are mapped at the top of the alignment. Trypanosome-specific inserts that block hexamer formation are labeled by magenta bars and the region of human UPP1 that is responsible for blocking hexamer formation is shaded pink. The blue box marks the hydrophobic patch important for dimer-dimer interactions that allow for the trimer of dimer organization of the prototypical hexameric NP-I subfamily. This region has been substituted by more hydrophilic residues in the trypanosomal and human homodimers. The UP-specificity region is marked by an orange bar and the key uridine recognition residues are highlighted in cyan. The metal coordinating residues of TbUP are marked with an “M” at the bottom of the sequences. The key substrate/product interacting residues are labeled “U” for uracil, “R” for ribose, and “P” for phosphate. The residues contributed by the neighboring monomer are lower-case and colored green rather than red. Structure-based sequence alignment was created using Expresso (3D-Coffee)[68] with some manual editing and the figure was prepared using TEXshade.[69] Tb, *T. brucei*; Hs, *Homo sapiens*; Ec, *E. coli*; Pf, *P. falciparum*; PDB codes used for the structural alignment follow the species-enzyme name. **(c)** Superposition of the TbUP dimer on the prototypical hexameric form of the NP-I family, in this case represented by the PNP from *Plasmodium falciparum* (PDBID 2bsx),[32] to highlight the consequence of the TbUP hexamer-blocking inserts. The view is equivalent to that in the right-hand picture of panel 1a; looking parallel to what would be the 3-fold symmetry axis of the trimer of dimers. The TbUP dimer is red with an orange UP-specificity region and magenta hexamer-blocking inserts. The equivalent *P. falciparum* dimer unit is green and the neighboring dimer of the hexamer is gray. The TbUP inserts that prevent hexamer formation sterically clash with the neighboring hexameric subunit. **(d) S**quare antiprism coordination environment of the intermolecular calcium ion. The coordination environment is shown as gray dashes and the coordination bonds are black lines with distances in angstroms. The coordinating residues are Met^{87}, Asp^{90}, and Asn^{91} contributed by each monomer, one colored green and the other cyan.

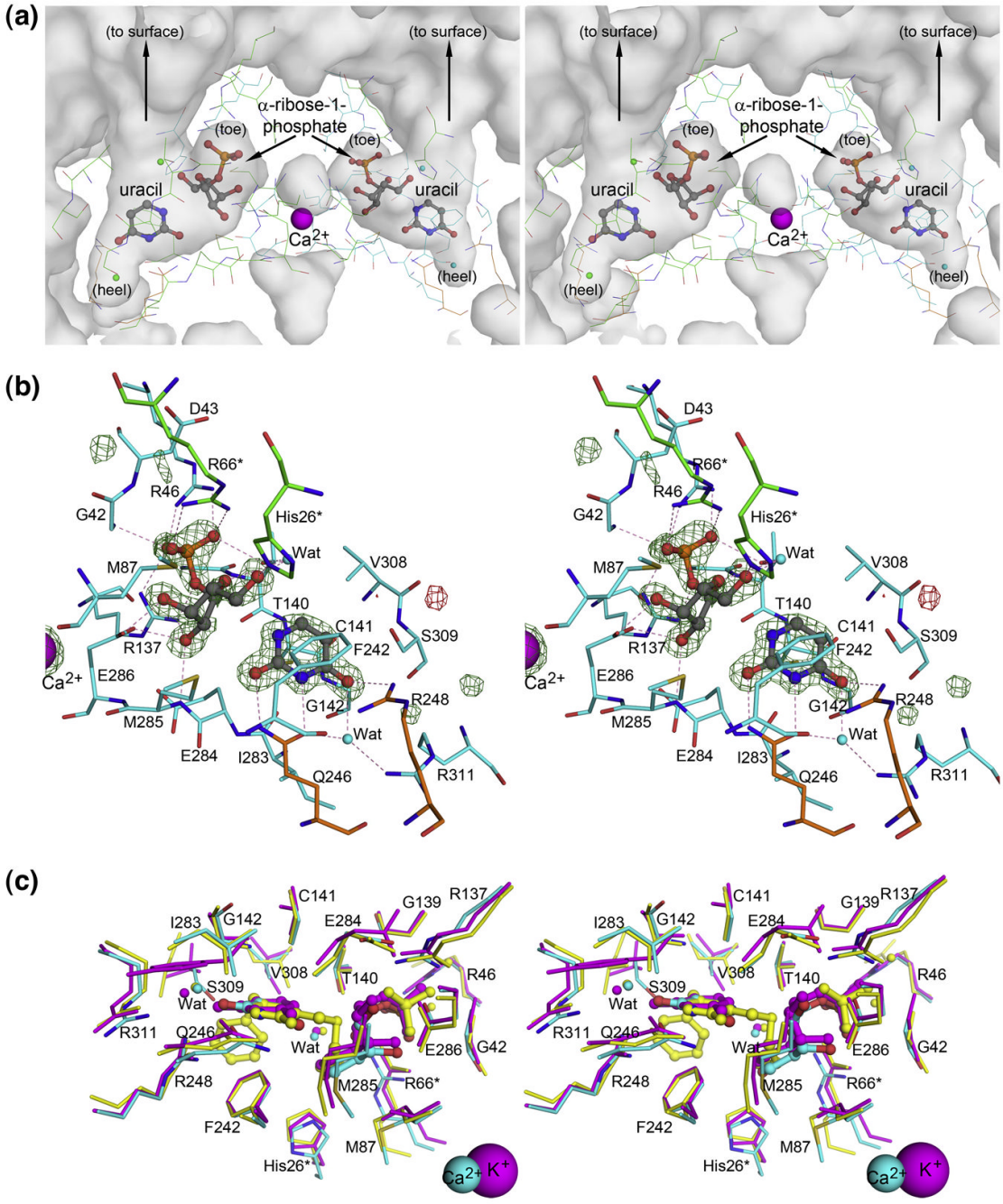

Figure 2.

Active site environment of TbUP. **(a)** The boot-shaped active site pockets are shown as a transparent surface and the products are shown as sticks. α-Ribose-1-phosphate and uracil are bound in the heel and the toe of the boot, respectively. Residues within 4 Å of the products or the intermolecular Ca^{2+} ion are shown as lines, colored cyan for one monomer and green for the second, with the exception of those in the UP-specificity region that are orange for both monomers. The view is rotated 100° around the Y-axis with respect to the view in the right-hand picture of panel 1a. **(b)** Stereo view of the active site environment around the products, uracil and α-ribose-1-phosphate, and calcium ion. The sigmaA-weighted[70] Fo-Fc electron density map (mesh) was calculated with products and the calcium ion omitted from the model

and is contoured at +5σ (green mesh) and −5σ (red mesh). The view is zoomed in on the products from the right-hand monomer of panel 2a. Amino acids within 4A of the products are shown as sticks and colored according to the monomer they come from as in panel 2a. Hydrogen bonds are shown as dashed pink lines. **(c)** Superposition of the ligand-bound active sites of TbUP with EcUP (PDB 1tgy) and HsUPP1 (PDB 3euf). The side chains of residues (or whole Gly residues) within 4 Å of the bound uracil and ribose-1-phosphate are shown as sticks with TbUP colored cyan, EcUP colored magenta, and HsUPP1 colored yellow. The ligands (uracil and ribose-1-phosphate for TbUP and EcUP and 5-benzylacyclouridine for HsUPP1) are shown as ball-and-sticks, metals and waters are shown as spheres, and are the same color as the enzyme for which they are bound. Structures were superimposed by SSM[71] in Coot.

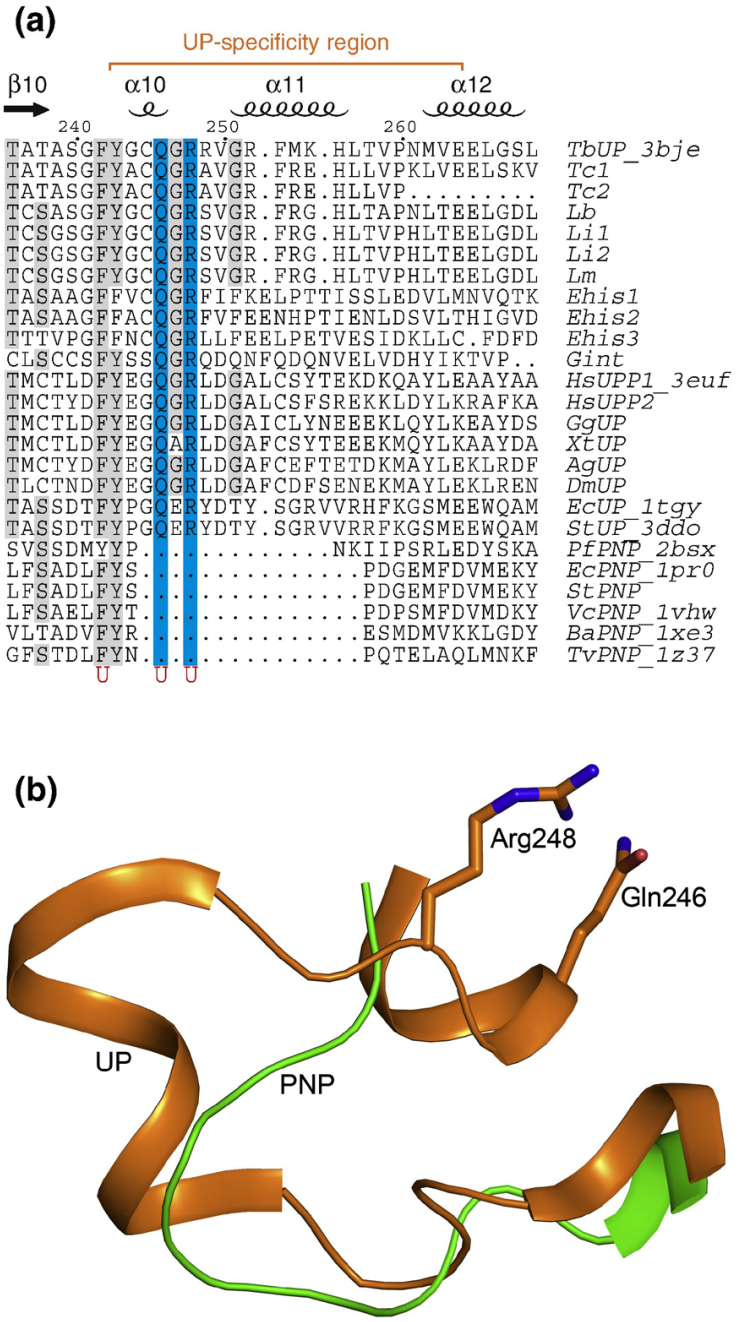

Figure 3.

Comparison of nucleoside phosphorylases in the vicinity of the UP-specificity region. **(a)** Sequence alignment of several characterized UP and PNP sequences with several uncharacterized putative nucleoside phosphorylase sequences from pathogenic protozoa of interest to MSGPP. The UP-specificity region is present in known UPs and is absent in known PNPs. The presence of this insert with the two key substrate discrimination residues (Gln and Arg) in many uncharacterized sequences strongly suggests that they possess UP activity. Alignment was created using Expresso (3D-Coffee)[68] with manual editing using the alignment in Figure 1b as a guide. **(b)** Structural comparison of the backbone trace of the UP-specificity region. TbUP (PDBID 3bje), is colored orange and the structurally aligned counterpart from

P. falciparum PNP (PDBID 2bsx) is colored green. The key substrate discriminating residues, Gln^{246} and Arg^{248}, are shown as sticks for TbUP and PfPNP has no equivalent residues.

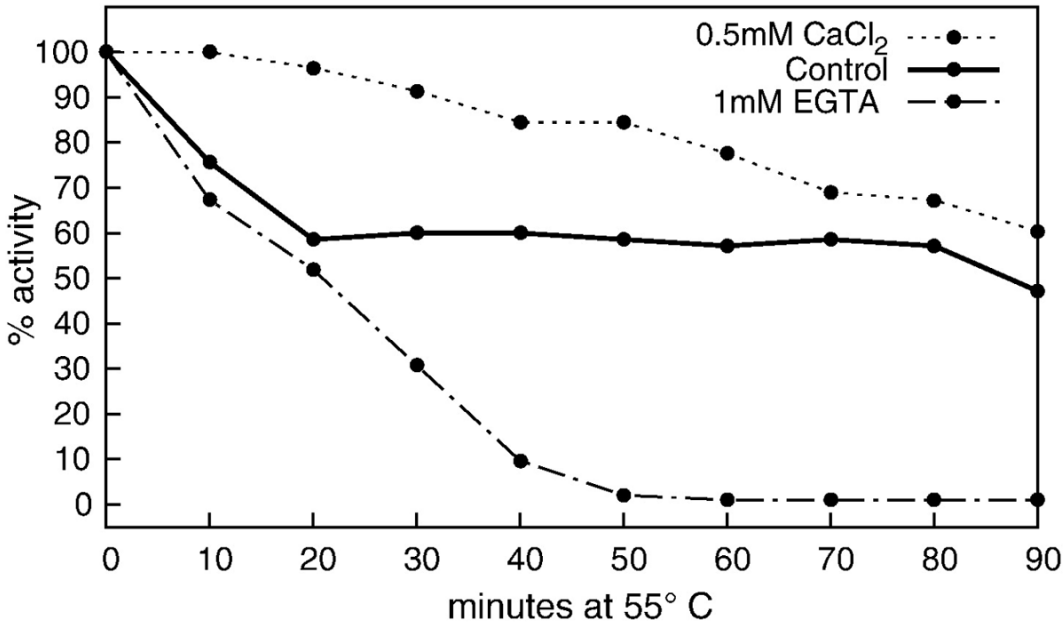

Figure 4.

Effect of Ca^{2+} on TbUP stability. TbUP activity was monitored over time at elevated temperature in the presence of EGTA or $CaCl_2$ to assess if the intermolecularly-bound Ca^{2+} observed in the crystal structure contributes to enzyme stability. The reaction buffer was not supplemented with EGTA or $CaCl_2$ for the control experiment. The rapid loss of enzyme activity in the presence of EGTA compared to the gradual loss of activity in the presence of Ca^{2+} suggests that the metal ion stabilizes the catalytically active form of the TbUP. Activity is plotted as a percentage of the initial activity at time point 0.

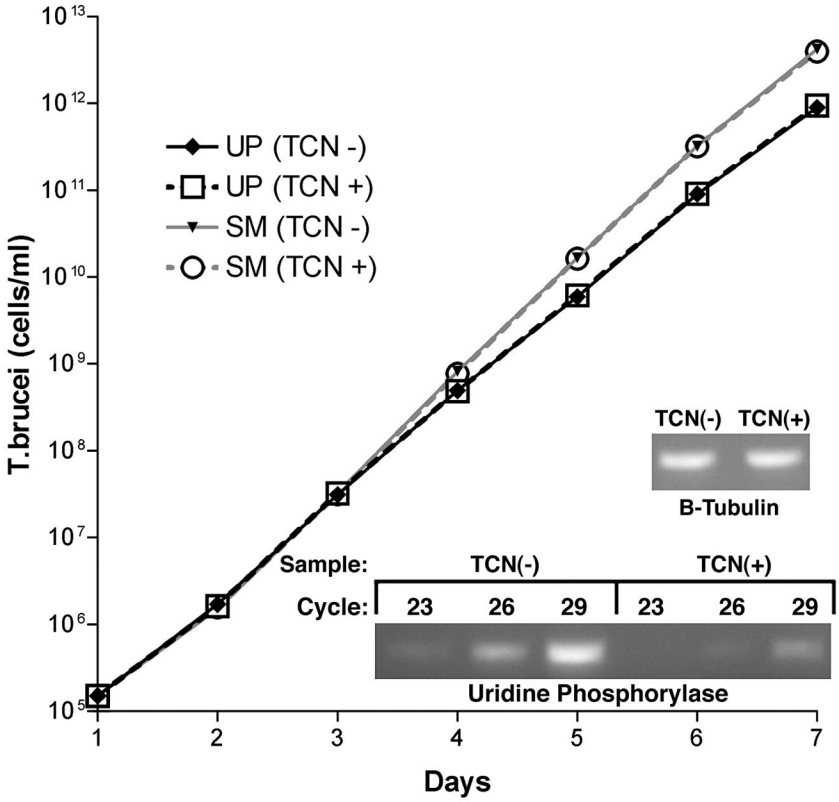

Figure 5.

Gene knockdown of *T. brucei* UP using RNA interference. Cumulative cell densities are shown on a log-scale as the product of the cell number and the total dilution. *T. brucei* undergoing RNAi of UP (TCN+) is compared to cells without RNAi induction (TCN−). The growth rate was also compared with the 'single marker' (SM) strain of *T. brucei* that was not transfected with the RNAi expression vector (semi-logarithmic plot). Knockdown of *T. brucei* mRNA expression 72 h after induction of RNAi with tetracycline was demonstrated by PCR of cDNA at cycles 23, 26 and 29 and visualized by ethidium bromide stain of agarose gel (lower inset). Even loading was demonstrated by PCR of the β-tubulin gene (upper inset).

Table 1

Data collection statistics[a]

Dataset	Se peak	Se remote	Uridine cocrystal
Beamline	SSRL 9-2		SSRL 9-2
Spacegroup	$P2_1$		$P2_1$
Unit cell parameters (a, b, c, β, α=γ=90°)	63.1 Å, 95.6 Å, 63.5 Å, 105.9°		63.1 Å, 95.4 Å, 63.5 Å, 105.9°
Resolution (Å)	50-2.27 (2.35-2.27)		40-1.44 (1.50-1.44)
Wavelength (Å)	0.9791	0.9116	0.917
Unique reflections	31,735	22,922	123,263
Completeness (%)	95.1 (77.8)	71.0 (65.1)	95.4 (73.4)
R_{merge}	0.11 (0.30)	0.09 (0.38)	0.08 (0.64)
Mean $I/\sigma(I)$	10.0 (2.8)	8.1 (1.8)	8.4 (1.2)
Redundancy	3.3 (3.0)	2.3 (2.4)	3.4 (2.4)
Wilson B factor (Å^2)	26.7		15.8

[a] Values in parenthesis are for the highest resolution shell.

Table 2

Model refinement statistics

Dataset	Uridine cocrystal
Resolution (Å)	35.4-1.44
R_{work}	0.155
R_{free}	0.184
No. reflections; refinement/test set	123,193/6,191
RMSD bonds (Å)	0.01
RMSD angles (°)	1.3
Protein atoms	5,047
Nonprotein atoms	554
Residues in favored regions (%)[a]	97.9
Residues in allowed regions (%)[a]	100
Unmodeled residues	−7 to 14 for both chains
TLS groups (residues)[b]	A chain: 15-63, 64-106, 107-118, 119-145, 146-174, 175-196, 197-227, 228-257, 258-309, 310-319, 320-341; B chain: 15-21, 22-105, 106-113, 114-145, 146-175, 176-191, 192-224, 225-253, 254-283, 284-313, 314-341
Mean B_{iso} + B_{TLS} protein atoms (Å ^{2})	23.9
Mean B_{iso} catalytic product atoms (Å^2)	22.0
Mean B_{iso} metal atom (Å ^{2})	13.0
Mean B_{iso} solvent atoms (Å ^{2})	32.4
PDB code	3BJE

[a] Determined using the MolProbity Server.[57]

[b] Selected with the aid of the TLSMD server.[55]

Table 3

Substrate specificity

Substrate	Activity (μmole/mg/min)[a]	Relative Activity (%)
Uridine	2.81±0.30	100
Deoxyuridine	0.40±0.03	14
Thymidine	< 0.04	< 1.4
Cytidine	< 0.001	< 0.03
Deoxycytidine	< 0.001	< 0.03
Inosine	< 0.001	< 0.03
Adenosine	< 0.15	< 5.0
Deoxyadenosine	< 0.2	< 7
Guanosine	< 0.3	< 10
Deoxyguanosine	< 0.2	< 7

[a] reactions at 25 °C, pH 7.5

Table 4

Effect of pH on UP activity

	Activity (μmole/mg/min)[a]	
pH	**Uridine**	**Deoxyuridine**
6.0	1.70±0.46	1.44±0.06
6.5	1.86±0.29	1.55±0.27
7.0	1.91±0.39	0.64±0.10
7.5	2.75±0.32	0.44±0.07
8.0	2.68±0.34	0.22±0.15
8.5	1.55±0.24	0.13±0.08

[a] reactions at 25 °C